Past and Projected Changes in Western North Pacific Tropical Cyclone Exposure

JAMES P. KOSSIN

NOAA/National Centers for Environmental Information, Asheville, North Carolina

KERRY A. EMANUEL

Massachusetts Institute of Technology, Cambridge, Massachusetts

SUZANA J. CAMARGO

Lamont-Doherty Earth Observatory, Columbia University, Palisades, New York

(Manuscript received 18 January 2016, in final form 6 May 2016)

ABSTRACT

The average latitude where tropical cyclones (TCs) reach their peak intensity has been observed to be shifting poleward in some regions over the past 30 years, apparently in concert with the independently observed expansion of the tropical belt. This poleward migration is particularly well observed and robust in the western North Pacific Ocean (WNP). Such a migration is expected to cause systematic changes, both increases and decreases, in regional hazard exposure and risk, particularly if it persists through the present century. Here, it is shown that the past poleward migration in the WNP has coincided with decreased TC exposure in the region of the Philippine and South China Seas, including the Marianas, the Philippines, Vietnam, and southern China, and increased exposure in the region of the East China Sea, including Japan and its Ryukyu Islands, the Korea Peninsula, and parts of eastern China. Additionally, it is shown that projections of WNP TCs simulated by, and downscaled from, an ensemble of numerical models from phase 5 of the Coupled Model Intercomparison Project (CMIP5) demonstrate a continuing poleward migration into the present century following the emissions projections of the representative concentration pathway 8.5 (RCP8.5). The projected migration causes a shift in regional TC exposure that is very similar in pattern and relative amplitude to the past observed shift. In terms of regional differences in vulnerability and resilience based on past TC exposure, the potential ramifications of these future changes are significant. Questions of attribution for the changes are discussed in terms of tropical belt expansion and Pacific decadal sea surface temperature variability.

1. Introduction and motivation

Over the past few decades, the average location where tropical cyclones (TCs) reach their peak lifetime intensity has systematically migrated poleward in some regions (Kossin et al. 2014). This has occurred concurrently with systematic changes in the mean tropical and subtropical environments (Kossin et al. 2014; Kang and Elsner 2016). Statistically significant poleward migration rates in the mean latitude where TCs reach their lifetime-maximum intensity (LMI; denoted herein as ϕ_{LMI}) are observed in the western North Pacific Ocean (WNP), southern Indian Ocean, and South Pacific Ocean, with statistically insignificant rates found in the eastern North Pacific and northern Indian Oceans and a statistically significant equatorward migration rate in the North Atlantic (Fig. 1). In a hemispheric sense, then, TCs in both the southern Indian and South Pacific Oceans apparently contribute to the observed poleward migration in the Southern Hemisphere, while WNP TCs contribute largely to the Northern Hemisphere trends identified by Kossin et al. (2014). The WNP is the most active ocean basin in terms of TC activity and also encompasses most regions with the highest human exposure and mortality risk from TCs (Peduzzi et al. 2012). In particular, there is a large amount of coastline poleward of the tropics in the WNP

Corresponding author address: James Kossin, NOAA/Cooperative Institute for Meteorological Satellite Studies, 1225 West Dayton St., Madison, WI 53706.
E-mail: james.kossin@noaa.gov

DOI: 10.1175/JCLI-D-16-0076.1

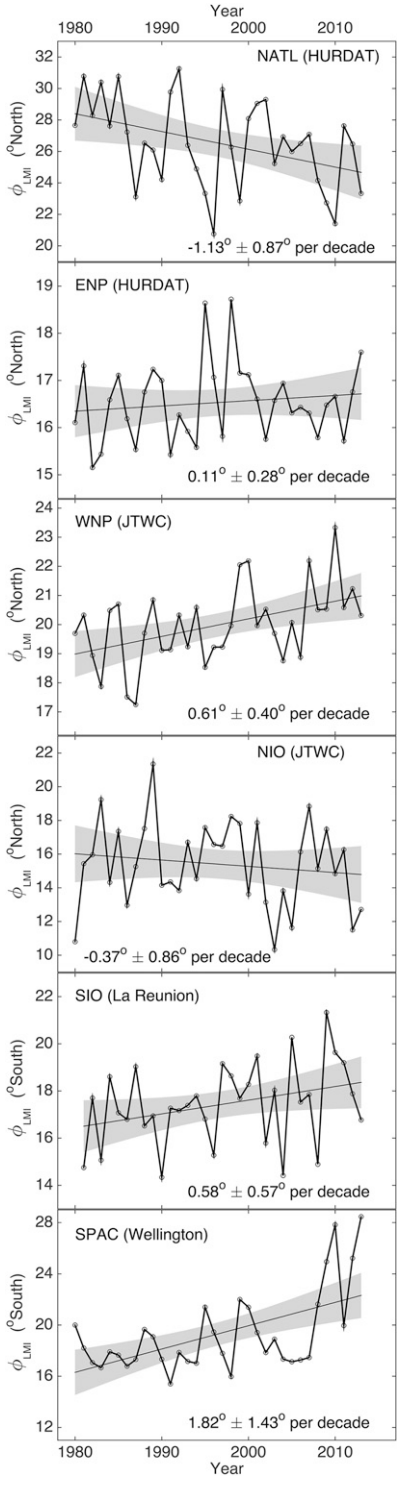

FIG. 1. Time series (°lat decade^{-1}) of annually averaged ϕ_{LMI} using best-track data from the six ocean basins that support TCs: the North Atlantic (NATL), eastern and western North Pacific (ENP and WNP), northern and southern Indian (NIO and SIO), and South Pacific (SPAC). Best-track data sources used here for these ocean basins are HURDAT, JTWC, La Réunion, and Wellington (Knapp et al. 2010). Shading shows 95% confidence bounds. Annotated values represent the mean migration rates and their 95% confidence intervals (° decade^{-1}).

that is exposed to TC-related hazard. Contrarily, while the southern Indian and South Pacific Oceans experience a relatively high level of TC activity, there is generally low hazard and mortality risk and limited coastline poleward of the tropics (Peduzzi et al. 2012).

Any systematic regional changes in WNP TC exposure associated with decadal TC track migration would be highly problematic for a number of reasons. In addition to TC-related human risk factors brought by wind, storm surge, and extreme rainfall, many regions depend on TC passage for their freshwater supply (Jiang and Zipser 2010; Lam et al. 2012). In this case, the benefits of reduced TC exposure need to be tempered by the potential for potable water shortages. Regional changes in TC exposure also need to be considered in light of differing regional sensitivities to TC hazards. For example, the sensitivity to typhoons on Guam, in the Marianas, is relatively small because of local building codes (many homes in Guam are built similarly to concrete bunkers), warning systems, and public education based on the experience that climatologically high TC exposure has brought to the region. Contrarily, regions that experience comparatively low climatological TC exposure, such as Japan for example, can be more sensitive to TC hazards and impacts because of a comparative lack of experience-based adaptation strategies (Cardona et al. 2012). Increasing TC exposure in these regions has the potential to significantly increase vulnerability and, consequently, mortality risk. All of these aspects indicate a need for a more in-depth exploration of WNP TC track and exposure changes, both past and projected.

In this paper, we explore intrabasin changes in WNP TC track characteristics using a combination of observations and numerical model simulations from phase 5 of the Coupled Model Intercomparison Project (CMIP5; Taylor et al. 2012). Section 2 discusses the data and methods applied in the subsequent sections. In section 3, historical TC data from the four sources that provide best-track data in the WNP since 1980 are analyzed with a focus on regional changes in TC exposure patterns. Taking advantage of the fact that ϕ_{LMI} is comparatively insensitive to heterogeneities in the best-track data (Kossin et al. 2014), TC track variability is then considered over longer time periods in light of known modes of interannual and decadal variability in an attempt to disentangle natural and anthropogenic causes for the observed migration. In section 4, we explore twenty-first-century projections of WNP TC track and exposure variability simulated by, and downscaled from, an ensemble of numerical CMIP5 models. The paper concludes with a summary and discussion in section 5.

2. Data and methods

Observational TC data were taken from the International Best Track Archive for Climate Stewardship (IBTrACS), version 03r06, which provides estimates of TC center position and intensity every 6 h during the lifetime of each TC (Knapp et al. 2010). There are four best-track data sources from four distinct agencies in the WNP: the Joint Typhoon Warning Center (JTWC), Japan Meteorological Agency (JMA), China Meteorological Administration (CMA), and Hong Kong Observatory (HKO). We note here that these four sources often differ, sometimes substantially, in their reported values for the same TCs, but they are not likely to be completely independent and their ensemble does not necessarily represent four unique datasets. Lifetime-maximum intensity is the peak intensity reached by each TC during its lifetime (Elsner et al. 2008). Best-track data provide intensities in units of knots (kt; $1\,\text{kt} \approx 0.51\,\text{m}\,\text{s}^{-1}$). The latitude where LMI is reached is denoted herein as ϕ_{LMI}. Only TCs with LMI ≥ 35 kt are used in the following analyses.

As introduced in Kossin et al. (2014), the metric ϕ_{LMI} is comparatively robust to the heterogeneities introduced into best-track data by both temporal inconsistency in data quality and analysis as well as interagency procedural differences. For example, ϕ_{LMI} is insensitive to the differences in wind-averaging techniques because it does not consider intensity in an absolute sense but only requires identifying when and where the maximum intensity occurs relative to a TC's lifetime; that is, ϕ_{LMI} is unaffected by procedural heterogeneities across the different best-track data sources. The metric ϕ_{LMI} is also comparatively insensitive to the usual temporal heterogeneities of intensity estimates, again because the absolute value of intensity is not needed; rather, only knowledge that a maximum intensity was achieved for that particular TC is necessary (ϕ_{LMI} represents only the latitude at that time). In the case of ϕ_{LMI}, the well-known and substantial temporal heterogeneities in absolute intensity estimates that have been introduced into the best track by numerous changes in technology play a much smaller role. Whatever technology is applied in a given era, it will not systematically change during a TC's lifetime, and the ability to identify the LMI, whatever its absolute value is, should remain similar as technology changes. The metric ϕ_{LMI} simply marks the latitude at that moment of a TC's lifetime.

TC exposure is expressed in terms of track density on a $2° \times 2°$ latitude–longitude grid in units of ensemble-average number of days per year that a TC center was in that grid box. In the model projection ensembles, the WNP is defined as the region north of the equator and within 100°E–180° longitude.

Monthly indices of El Niño–Southern Oscillation (ENSO) and the Pacific decadal oscillation (PDO) are provided by NOAA's Earth System Research Laboratory Physical Sciences Division[1] (Rayner et al. 2003; Mantua et al. 1997). Annual averages of the indices were taken over July–November (JASON), which comprise the months of greatest WNP TC activity (about 80% of annual TC genesis events occurs in these months). ENSO and PDO variability was removed from the time series of annual-mean ϕ_{LMI} by regressing ϕ_{LMI} onto their annual-mean index values and forming time series of the residuals of the regressions.

The TCs explicitly simulated by the CMIP5 models are the same as described in Camargo (2013), and the ''synthetic'' TCs that were downscaled from CMIP5 model output are the same as those described in Emanuel (2013, 2015). Here we have 100 synthetic TCs per year to sample from. Relative annual frequencies are determined by the percentage of random vortex seeds that reach a specified intensity threshold in the downscaling technique (Emanuel et al. 2008).

None of the time series analyzed here exhibits autocorrelation as determined by a Durbin–Watson test statistic, with the exception of the Wellington best-track data time series shown in Fig. 1. The Wellington time series confidence bounds were corrected to account for this. No other adjustments were stipulated.

3. Observed changes in WNP ϕ_{LMI} and associated changes in TC exposure

The poleward migration of ϕ_{LMI} in the WNP shown in Fig. 1 is consistent across the four best-track data sources available for that region (Fig. 2), which, when considered in concert with the temporal and interagency robustness of the metric ϕ_{LMI}, provides high confidence in the fidelity of the mean migration rate. On average, ϕ_{LMI} has migrated poleward in the WNP at a rate of $0.56° \pm 0.40°$ decade^{-1} in the period 1980–2013[2]. Associated with this change in mean ϕ_{LMI} is a pronounced and nearly uniform poleward shift in the distribution of ϕ_{LMI} (Fig. 3). While the mean ϕ_{LMI} increases by only about 2° latitude in the past 34 years, the changes in the tails of the distribution can be large and the probability of a TC reaching peak intensity at the lowest (highest)

[1] Available from http://www.esrl.noaa.gov/psd/gcos_wgsp/Timeseries/Nino34/ and http://www.esrl.noaa.gov/psd/gcos_wgsp/Timeseries/PDO/, respectively.

[2] Using a record of homogenized TC intensity presently available within the period 1982–2009 (Kossin et al. 2013), ϕ_{LMI} has migrated poleward in the WNP at a rate of $0.94° \pm 0.64°$ decade^{-1}.

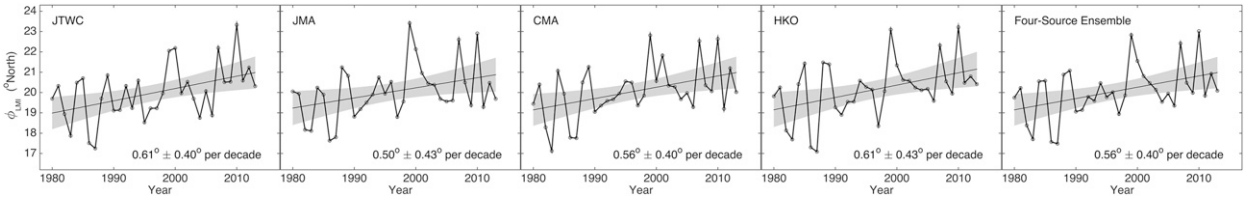

FIG. 2. As in Fig. 1, but for best-track data from the four WNP sources—JTWC, JMA, CMA, and HKO—and an ensemble of the four sources.

latitudes have proportionally become substantially smaller (greater) in this time period.

In the postgeostationary satellite period of highest-quality TC data, since around 1980, the overall frequency of WNP TCs has decreased by around 15% (from an average of about 27–28 yr^{-1} over 1980–96 to about 23–24 yr^{-1} over 1997–2013) leading to a general decrease in basinwide TC exposure (Liu and Chan 2013; Yokoi and Takayabu 2013; Lin and Chan 2015). Over this same period, however, the changing distribution of ϕ_{LMI} has been associated with a change in WNP TC track characteristics in general (e.g., Chu et al. 2012), and the combined effects of basinwide frequency changes and track changes have caused substantial changes in regional TC exposure through changes in track density (Fig. 4). In the more southern regions of the Philippine and South China Seas, the combined effects of the basinwide reduction in TC frequency and the poleward migration has led to a large reduction in TC exposure. In more northern regions, in and around the East China Sea, the basinwide reduction has been offset by the poleward migration. The TC exposure around the Marianas and the Philippines in particular has decreased substantially, by around 50% or more, in the latter half of the period 1980–2013. Contrarily, exposure in the regions of Japan and its Ryukyu Islands, the Korea Peninsula, and Taiwan has increased, by as much as 100% or more in some regions, despite the overall reduction in basinwide TC counts.

On interannual time scales, TC tracks are substantially modulated by the natural variability of ENSO. This modulation occurs in the North Atlantic (Kossin et al. 2010), the eastern North Pacific (Camargo et al. 2008), the Southern Hemisphere (Ramsay et al. 2012), and, of relevance to this study, the WNP (Camargo et al. 2007; Zhao et al. 2010; Goh and Chan 2012; Zhang et al. 2012; Wang and Wang 2013). This variability, however, does not project onto the decadal time scale of global TC migration (Kossin et al. 2014). For the particular case of WNP TCs, this is further demonstrated in Table 1, which shows the statistics of regressions of annual-mean ϕ_{LMI} from each data source onto the JASON average of a Niño-3.4 index and compares migration rates with and without ENSO variability included. The JASON-mean Niño-3.4 index explains 24%–43% of the interannual variance of ϕ_{LMI} and the regression coefficient is statistically significant for each data source. However, when ENSO variability is removed from the time series of annual-mean ϕ_{LMI}, the migration rates are only minimally affected while the uncertainty in the rates actually decreases substantially (cf. the migration rates of ϕ_{LMI} and the regression residuals $\varepsilon_{\text{Niño-3.4}}$ in Table 1). That is, ENSO variability simply adds noise to the ϕ_{LMI} time series but does not project onto the migration rate.

The tracks of WNP TCs are also systematically modulated on decadal time scales by various modes of Pacific decadal variability such as the Pacific decadal oscillation (Ho et al. 2004; Liu and Chan 2008; Zhao and Wu 2014; Mei et al. 2015), which raises questions about whether the observed migration is part of a natural decadal cycle or a response to anthropogenic forcing (or, more plausibly, some combination of the two). To explore this with much confidence requires a longer time period than 1980–2013, which is fortunately possible with the available WNP best-track data. The data from the JTWC,

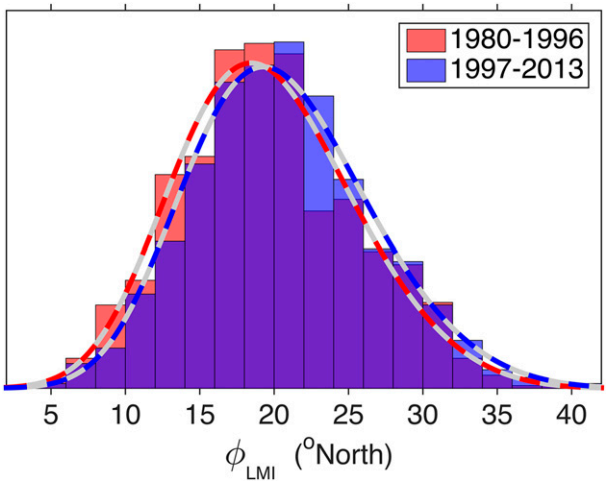

FIG. 3. Empirical probability density histograms of the four-source ensemble ϕ_{LMI} for the early (red) and later (blue) periods of analysis and their associated theoretical probability density functions (red and blue dashed curves).

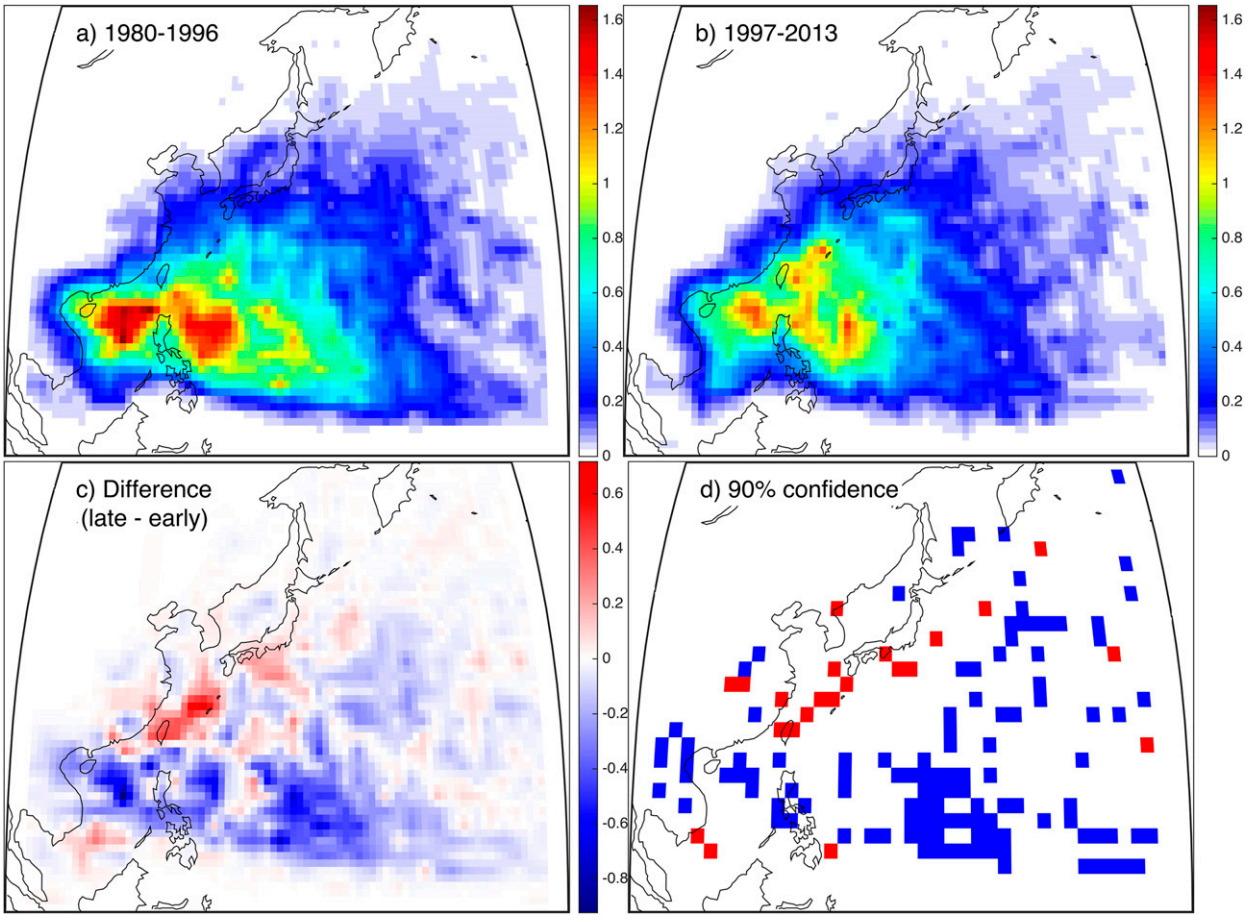

FIG. 4. Observed WNP TC track density (ensemble-average number of days of exposure per year per 2° × 2° latitude–longitude grid box) in the (a) early and (b) later halves of the observed period 1980–2013, and (c) the difference between them, for the four-source ensemble. (d) Regions where the differences between periods are significant at the 90% confidence level, based on a two-sided Student's *t* test, are colored red (blue) where exposure has significantly increased (decreased). Track density values in (a)–(c) are slightly smoothed with linear interpolation for better display clarity.

CMA, and HKO begin in years 1945, 1949, and 1961, respectively (JMA best-track data begin in 1979). Analysis of the earlier presatellite data should, in general, proceed with some caution because of the potential for data inaccuracies (e.g., Kossin et al. 2013), but we can proceed here with a reasonable level of confidence for three reasons: 1) prior to 1987, WNP TCs were routinely sampled by aircraft reconnaissance (Martin and Gray 1993), which significantly increases the accuracy of the earlier presatellite best-track data; 2) there are multiple

TABLE 1. WNP migration rates and 95% confidence intervals (°N decade^{-1}) of annual-mean ϕ_{LMI}, the residuals of the regression of ϕ_{LMI} onto the JASON-mean Niño-3.4 index (i.e., $\varepsilon_{\text{Niño-3.4}}$), and the residuals of the bivariate regression of ϕ_{LMI} onto the JASON-mean Niño-3.4 and PDO indices (i.e., $\varepsilon_{\text{Niño-3.4, PDO}}$) for the four WNP best-track data sources. For the single-variate regression, the variance explained R^2 and the p value are also shown. For the bivariate regression, the variance explained and the period of the available best-track data are shown. The ϕ_{LMI} and $\varepsilon_{\text{Niño-3.4}}$ time series span the period 1980–2013. No ensemble was calculated for the $\varepsilon_{\text{Niño-3.4, PDO}}$ time series because of the disparate periods of analysis for each source.

	JTWC	JMA	CMA	HKO	Ensemble
ϕ_{LMI}	0.61° ± 0.40°	0.50° ± 0.43°	0.56° ± 0.40°	0.61° ± 0.43°	0.56° ± 0.40°
$\varepsilon_{\text{Niño-3.4}}$	0.59° ± 0.34°	0.48° ± 0.33°	0.54° ± 0.34°	0.58° ± 0.30°	0.54° ± 0.30°
R^2, p value	0.24, 0.004	0.34, <0.001	0.24, 0.003	0.43, <0.001	0.35, <0.001
$\varepsilon_{\text{Niño-3.4, PDO}}$	0.21° ± 0.13°	Record too short	0.17° ± 0.16°	0.33° ± 0.19°	
R^2, period	0.24, 1945–2013		0.28, 1949–2013	0.34, 1961–2013	

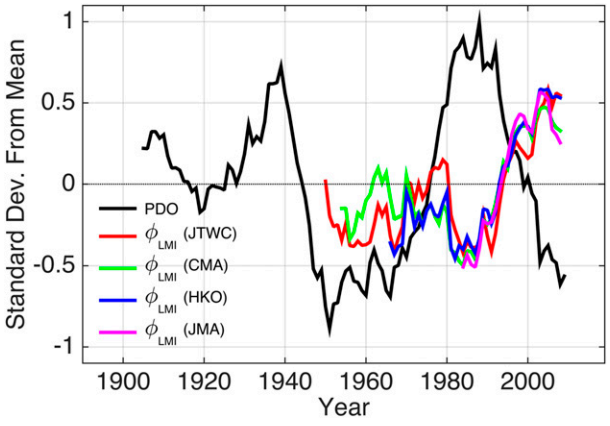

FIG. 5. Time series of smoothed annual-mean ϕ_{LMI} from each best-track data source (colored lines) and smoothed JASON-mean PDO index (black) as standard deviations from the mean. The available data from the JTWC, CMA, HKO, and JMA, respectively, begin in 1945, 1949, 1961, and 1979. PDO data extend back to 1900. Smoothing was applied with a running 11-yr centered mean, and the first and last 5 yr of each time series are not shown.

best-track data sources, which provides some measure of robustness/consistency testing; and 3) as noted earlier and discussed in Kossin et al. (2014), ϕ_{LMI} is comparatively less sensitive to best-track data heterogeneity.

The relationship between the decadal behavior of ϕ_{LMI} and the PDO is broadly demonstrated in Fig. 5, which shows an inverse relationship between the two [i.e., cool (warm) PDO phase is related to poleward (equatorward) location of peak TC intensity]. This is consistent with the previous studies noted above. Of particular relevance here is what part of the observed poleward TC migration is explained by known modes of Pacific decadal variability such as the PDO and what part, if any, may be related to other (possibly anthropogenic) forms of slow decadal forcing. Before we proceed with this exploration, it should also be noted that the decadal variability described by the smoothed PDO index is not tacitly internal or natural and very likely describes a conflation of natural and anthropogenic factors (Dong et al. 2014; Meehl et al. 2013; Boo et al. 2015). Furthermore, the expansion of the tropical belt, which Kossin et al. (2014) showed is consistent with the observed poleward TC migration, has been linked to both PDO variability and anthropogenic aerosol forcing (Allen et al. 2014), as well as various other factors, both natural and anthropogenic (Lucas et al. 2014).

In an attempt to disentangle the contributions of these factors to WNP TC migration and exposure changes, Fig. 6 shows time series of the residuals of annual-mean ϕ_{LMI} regressed onto indices of the PDO and ENSO. The multiple regression coefficients are statistically significant, as expected, and the JASON-mean PDO and Niño-3.4 indices together explain 24%, 28%, and 34% of the variability of annual-mean ϕ_{LMI} derived from the JTWC, CMA, and HKO best-track data, respectively (Table 1). When ENSO and PDO variability are removed (regressed) from the annual-mean ϕ_{LMI} time series, the residuals of the regression ($\varepsilon_{\text{Niño-3.4, PDO}}$ in Table 1) maintain a statistically significant poleward migration of 0.17°, 0.21°, and 0.33° decade^{-1}, respectively. This result is highly suggestive that the observed WNP TC migration can be attributed to a combination of natural and anthropogenic factors with a substantial portion of the migration occurring independently of the known dominant modes of variability in the region.

To further explore attribution linkages between anthropogenic forcing and WNP TC migration, the following section considers WNP TC behavior projected into the twenty-first century. Before we enter into that topic, it should be explicitly acknowledged that we have limited our discussion and analyses to questions of TC track variability and have not considered TC intensity variability in an absolute sense, although absolute intensity is clearly an important factor in assessing TC hazard and mortality risk. Introducing absolute intensity data into these analyses, whether from historical best-track records or from numerically simulated TCs,

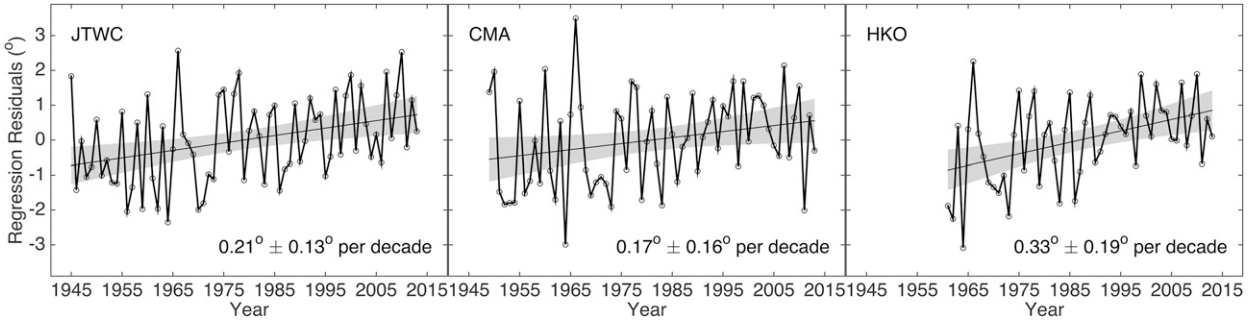

FIG. 6. As in Fig. 1, but for time series of residuals of the multivariate regression of annual-mean ϕ_{LMI} onto JASON-mean Niño-3.4 and PDO indices.

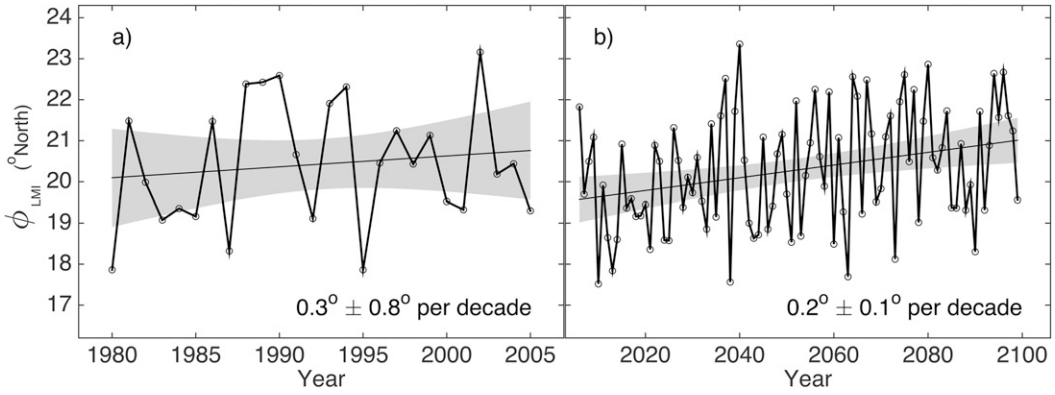

FIG. 7. As in Fig. 1, but for an ensemble of ϕ_{LMI} from WNP TCs explicitly generated in the 10 CMIP5 (a) historical and (b) twenty-first-century projection simulations.

introduces another layer of uncertainty (Kossin et al. 2013; Camargo and Wing 2016), and here we have chosen to focus only on the most robust metrics. Nonetheless, it should be noted that analysis of absolute intensity-based measures (e.g., TC power dissipation or simply mean intensity) shows similar patterns of change in both the best-track data and the model-based data discussed in the following sections. That is, there are no clear indications that absolute intensity changes have had or are projected to have any offsetting effects on the changes in track density and associated changes in TC exposure and risk explored here.

4. Projected changes in WNP ϕ_{LMI} and associated changes in TC exposure

If the observed poleward TC migration in the WNP is forced in part by anthropogenic factors, and consequently persists into the present century, then the associated changes in TC exposure would be expected to progressively impact various regions in the WNP. A number of previous studies have explored relationships between WNP TC track characteristics and anthropogenic climate change and have identified systematic shifts in TC genesis location and steering flow that combine to cause TC track shifts (Wu and Wang 2004; Li et al. 2010; Wang et al. 2011; Murakami et al. 2011, 2012; Yokoi et al. 2013; Bell et al. 2013; Mori et al. 2013; Manganello et al. 2014; Wu et al. 2014; Colbert et al. 2015; Mei et al. 2014, 2015; Roberts et al. 2015; Wang and Wu 2015). There is, however, some divergence among the model projections in some of these studies. While some high-resolution climate models (usually forced with fixed sea surface temperature) show a poleward shift that is generally attributed to the expansion of the tropics (e.g., Murakami et al. 2012; Wu et al. 2014), other modeling studies emphasize an eastward shift of the TC tracks toward the central Pacific (Li et al. 2010; Murakami et al. 2011; Yokoi et al. 2013; Mori et al. 2013). In some cases, northward and eastward shifts occur

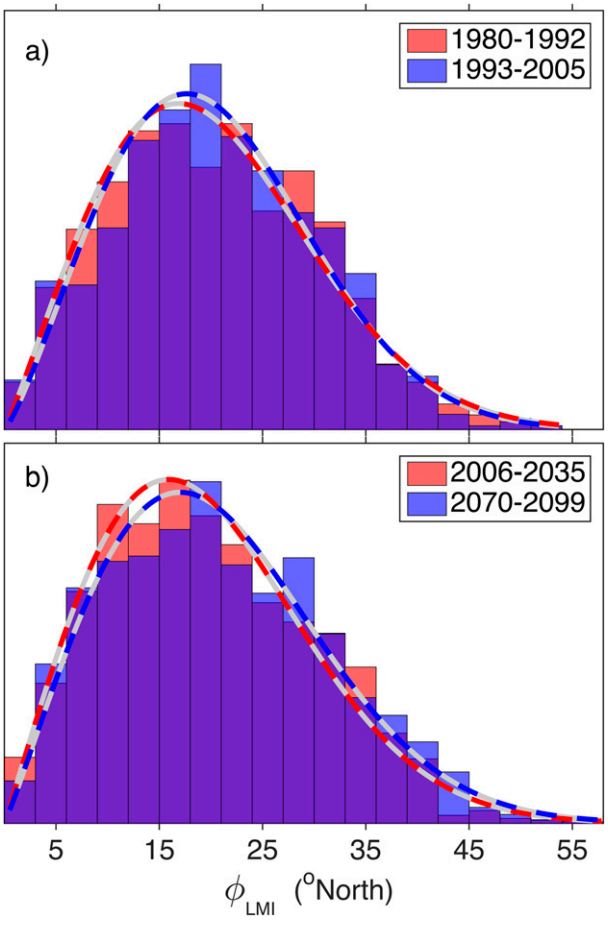

FIG. 8. As in Fig. 3, but for an ensemble of ϕ_{LMI} from WNP TCs explicitly generated in the 10 CMIP5 (a) historical and (b) twenty-first-century projection simulations. For the projected TCs, the first and last 30 years of the simulation are compared.

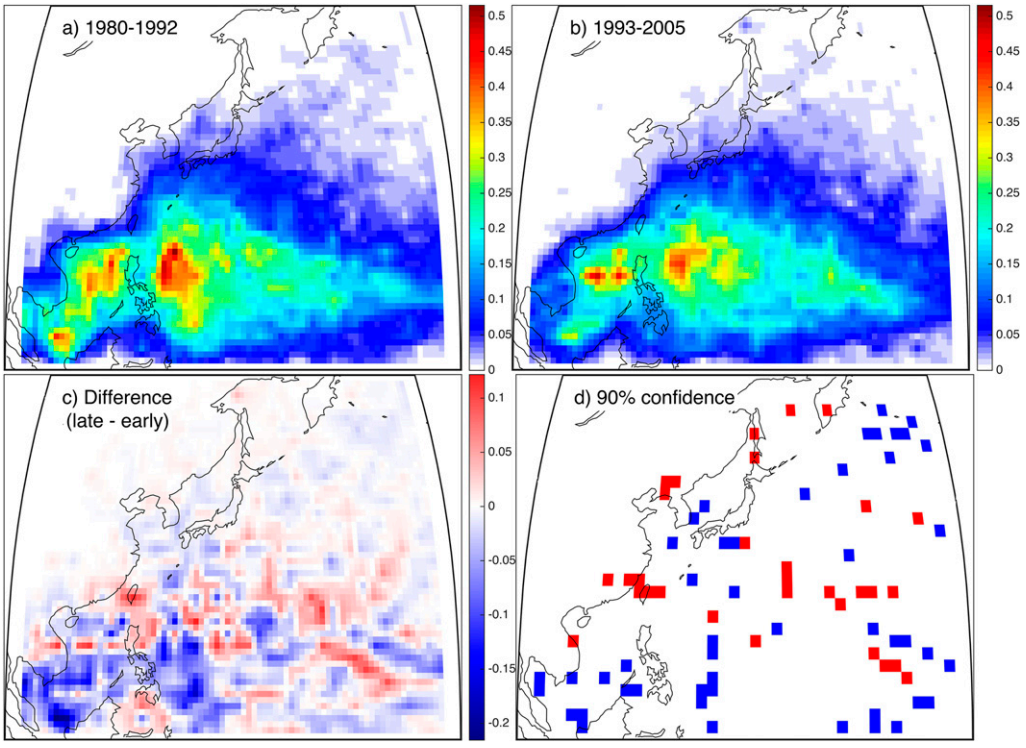

FIG. 9. As in Fig. 4, but for the ensemble of explicitly simulated TCs from the CMIP5 historical (1980–2005) simulations (note that the color scales differ from Fig. 4).

simultaneously as a northeastward migration (Murakami et al. 2012; Colbert et al. 2015; Roberts et al. 2015), and one model projects a southeastward shift (Manganello et al. 2014). While tempering our results with knowledge of this lack of firm consensus in model projections of WNP TC track variability, here we expand on previous work by analyzing the tracks of TCs formed in a suite of CMIP5 models (Camargo 2013) and downscaled from CMIP5 environmental data (Emanuel 2013, 2015), focusing on changes in ϕ_{LMI} and associated patterns of change of TC exposure, and comparing these patterns to observed patterns. Further tempering the interpretation of our results, a number of performance issues related to TCs generated by climate models or downscaled from climate model output have been documented (e.g., Camargo and Wing 2016; Emanuel 2015, and references therein). Here we will endeavor to present the model output as transparently as possible with the understanding that there are inherent uncertainties that exist.

a. TCs explicitly simulated by the CMIP5 models

Despite their relatively low spatial resolution, most of the CMIP5 models generate TC-like storms that can be tracked and analyzed. Here we use an ensemble of storms generated by 10 CMIP5 models, as described in Camargo (2013). The 10 models are described in Table 1 in Camargo (2013) with four models (INM-CM4.0, MIROC-ESM, MPI-ESM-LR, and NorESM1-M) omitted owing to a lack of TC generation in the WNP basin. The analyses here are applied first to CMIP5 historical simulations (1980–2005) for comparison with the observations and then to twenty-first-century projections under the representative concentration pathway 8.5 (RCP8.5) emissions scenario (Riahi et al. 2011).

In the historical simulations, the model ensemble tends to underestimate TC frequency, producing about 5.9 WNP TCs per year on average in the first half of the simulation period 1980–2005 and about 5.6 WNP TCs per year in the second half (roughly from one-fourth to one-fifth of the observed frequency). The underestimation of TC frequency is due, in part, to deficiencies in the models themselves, but there is also measurable sensitivity to the detection algorithm applied after the fact to the model output (Horn et al. 2014; Walsh et al. 2015). The rate of poleward migration and the poleward shift of the distribution of ϕ_{LMI} are also underestimated (cf. Figs. 7a and 8a to Figs. 2 and 3), although the general patterns of track density and track density change between the first and second halves of the period (Fig. 9) share some similarities with the observed changes (Fig. 4). If poleward TC migration is physically linked to the expansion of the tropics, the underestimation of the

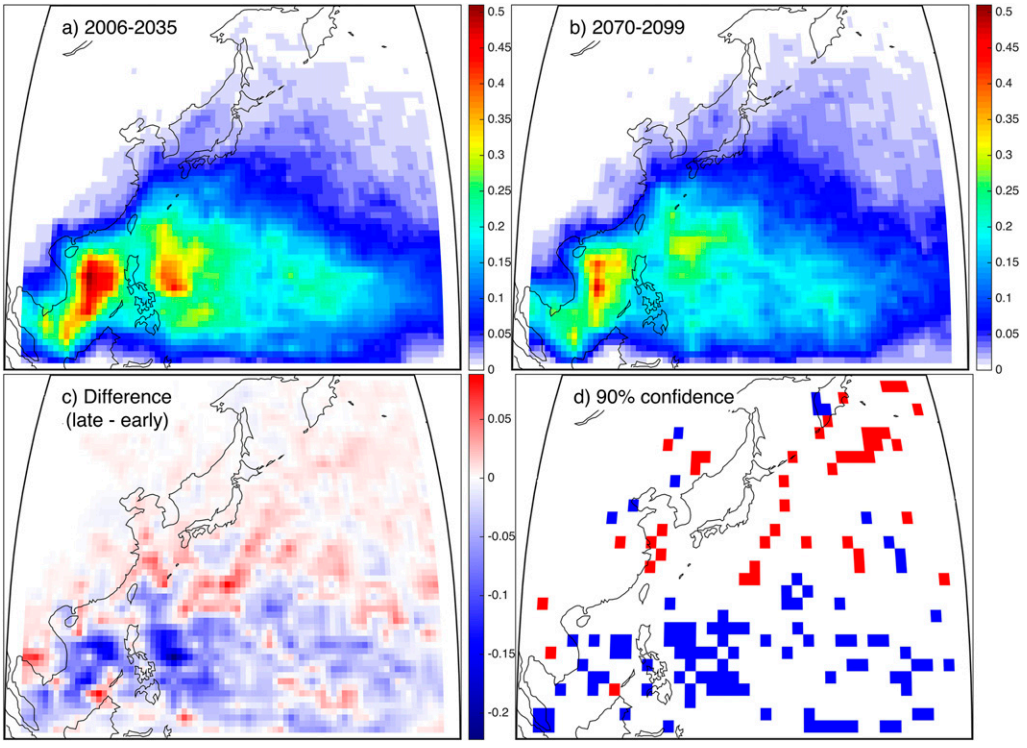

FIG. 10. As in Fig. 4, but for simulated changes in the track density of explicitly generated WNP TCs from the 10-member ensemble of CMIP5 projections in the first and last 30 years of the twenty-first century (note that the color scales differ from Fig. 4).

poleward migration in the historical simulations might be expected as the CMIP5 models have been independently shown to substantially underestimate the expansion of the tropical Hadley circulation (Hu et al. 2013; Nguyen et al. 2015).

In the twenty-first-century RCP8.5 projection simulations, the models again tend to underestimate TC frequency, producing an ensemble average of about 6.1 WNP TCs per year in the first 30 years of the simulation period 2006–99 and about 5.6 WNP TCs per year in the last 30 years. The projected reduction of WNP TC frequency is consistent with the general model consensus in that basin (Christensen et al. 2013, their Fig. 14.17). The projected rate of migration of annual-mean ϕ_{LMI} is about $0.2° \pm 0.1°\,\mathrm{decade}^{-1}$ (Fig. 7b), which is slower than the observed rate of about $0.56° \pm 0.40°\,\mathrm{decade}^{-1}$ in the period 1980–2013 (Fig. 2) but, interestingly, about the same as the observed poleward migration rate when ENSO and PDO variability are removed from the time series (Fig. 6). Similar to observations, the projected

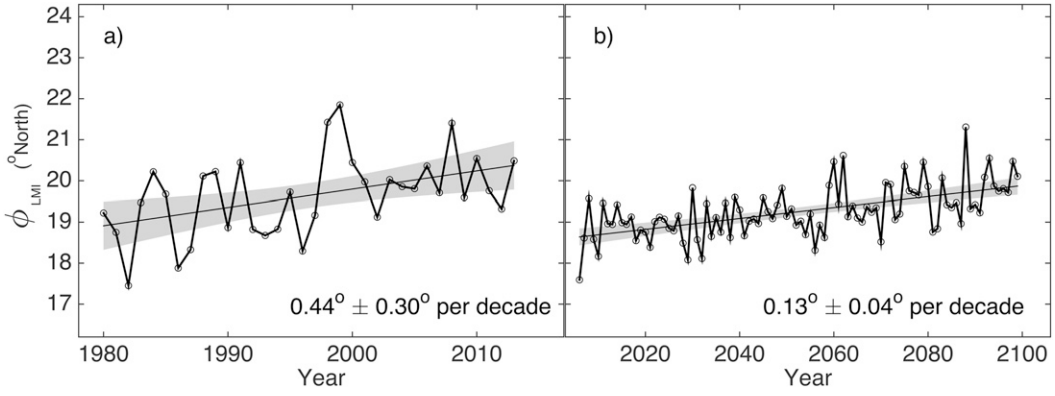

FIG. 11. As in Fig. 1, but for ϕ_{LMI} from WNP TCs downscaled from (a) reanalysis data and (b) model environmental data from eight CMIP5 twenty-first-century projection simulations.

poleward migration of annual-mean ϕ_{LMI} manifests within a fairly uniform poleward shift in the distribution of ϕ_{LMI} (Fig. 8b) and is associated with substantial changes in projected regional TC exposure (Fig. 10). The projected pattern of change of TC exposure is similar to the past observed changes (cf. Figs. 4 and 10), and the projected decrease in basinwide TC frequency either compounds or offsets the TC exposure changes as a result of track changes. Similar to the observed changes, in the regions of the Philippines and Marianas and regions surrounding the South China Sea, there are substantial projected decreases in exposure, by as much as 50% or more, in the last 30 years of this century compared to the first 30 years. Contrarily, the exposure in regions around the East China Sea, such as Japan and its Ryukyu Islands and the Korea Peninsula, is projected to increase despite the overall projected reduction in basinwide TC counts.

b. *TCs downscaled from CMIP5 model output*

In addition to TCs that are generated within the CMIP5 models, the CMIP5 model environmental fields can be downscaled to create large samples of synthetic TCs (Emanuel et al. 2006, 2008; Emanuel 2010). Here we use the global TC set described in Emanuel (2013, 2015) and repeat the analyses performed above using the WNP TCs. The downscaling method allows the generation of large numbers of synthetic TCs (for this study, we have 100 TCs per year to sample from), and the annual frequency is determined by the percentage of random vortex seeds that reach a specified intensity threshold (Emanuel et al. 2008). Similar to section 4a above, we use an ensemble of TCs downscaled from output from multiple CMIP5 models. The eight models used here are listed in Table 1 of Emanuel (2015) with the addition of NCAR's CCSM4.

Before analyzing the WNP TCs downscaled from the twenty-first-century CMIP5 model projections, we consider WNP TCs downscaled from past reanalysis data for comparison with the observations. The TCs are downscaled from the European Centre for Medium-Range Weather Forecasts (ECMWF) interim reanalysis (ERA-Interim; Dee et al. 2011) over the period 1980–2013. Here the observed mean annual frequency from the four best-track sources is used to sample the TCs from the larger sample of synthetic TCs. The time series of annual-mean ϕ_{LMI} from the downscaled WNP TCs (Fig. 11a) shows a significant poleward migration rate of about 0.44° ± 0.30° decade^{-1}, which is comparable but somewhat less than the mean observed rate of about 0.56° ± 0.40° decade^{-1} within the same period. The poleward shift of the distribution of ϕ_{LMI} is captured well by the TCs downscaled from the reanalysis data (cf. Fig. 12a to Fig. 3), and the pattern of change in TC exposure (Fig. 13) is broadly similar to the observed pattern of change (Fig. 4), with increased exposure in regions of the East China Sea and generally decreased exposure in the region around the northern Philippines (cf. Fig. 13 and Fig. 4). Similar results are found using data from the Modern-Era Retrospective Analysis for Research and Applications (MERRA; Rienecker et al. 2011) and the National Centers for Environmental Prediction–National Center for Atmospheric Research (NCEP–NCAR) reanalyses (Kalnay et al. 1996).

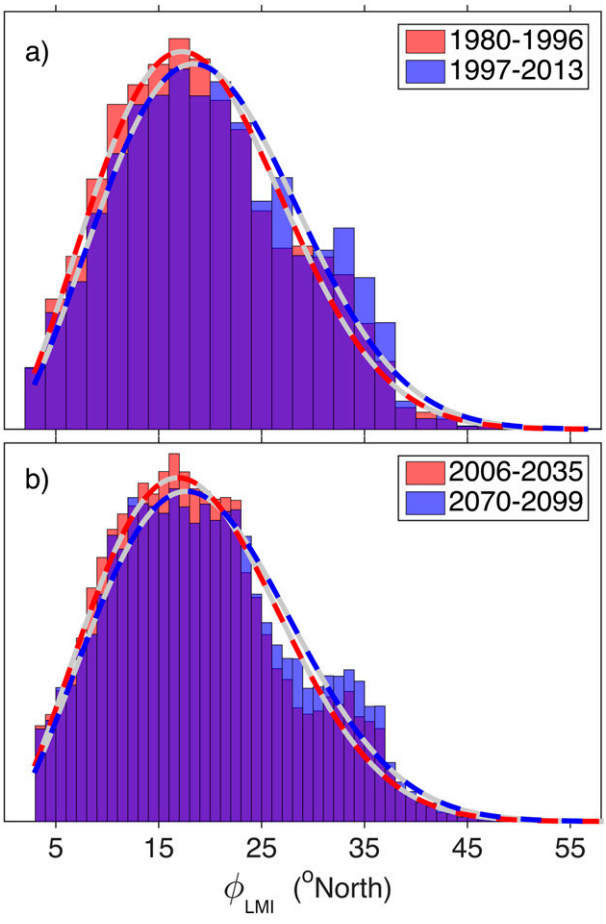

FIG. 12. As in Fig. 3, but for ϕ_{LMI} from WNP TCs downscaled from (a) reanalysis data and (b) model environmental data from eight CMIP5 twenty-first-century projection simulations.

When the same downscaling method is applied to the projected output from the eight CMIP5 models, a significant poleward migration of WNP ϕ_{LMI} emerges over the twenty-first century, with a rate of 0.13° ± 0.04° decade^{-1} (Fig. 11b), which is also associated with a poleward shift of the distribution of ϕ_{LMI} (Fig. 12b). The projected migration rate and interannual variability of ϕ_{LMI} in the downscaled TCs are smaller than found in

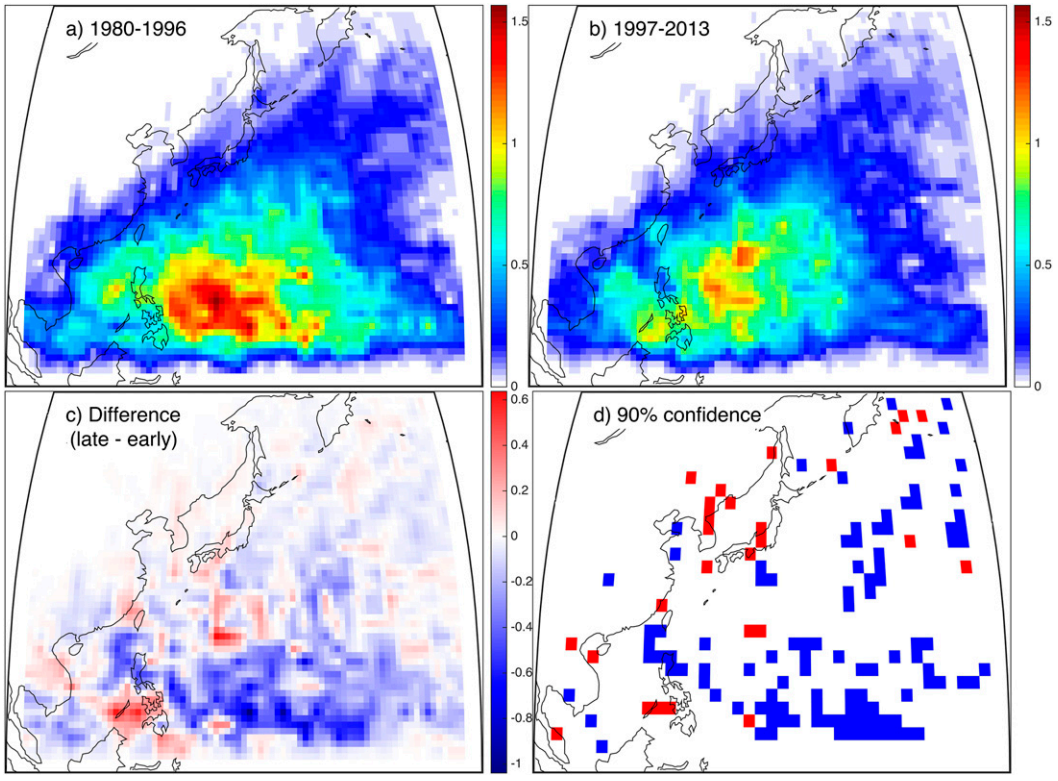

FIG. 13. As in Fig. 4, but for WNP TC tracks downscaled from reanalysis data.

the explicitly simulated TCs (for these analyses, the larger sample of available synthetic TCs are used, which is a likely factor in the reduced variance). As found in the explicitly simulated TCs, the poleward shift of ϕ_{LMI} is associated with regional changes in TC exposure. However, contrary to the explicitly simulated TCs, the projected frequency of the downscaled WNP TCs increases over the twenty-first century (Emanuel 2013), which causes a widespread and significant increase across the entire basin (Fig. 14). The increase in basin-wide frequency is substantial (about 22% when comparing the first and last 30 years of the simulation) and dominates the TC exposure changes due to track changes. To better separate the effect of the track and frequency changes, Fig. 15 shows the projected changes in TC exposure with annual frequency held fixed. When this is done, the patterns of exposure change due to track migration are found to be qualitatively similar to those of the explicitly simulated TCs, although with some quantitative differences.

An observed characteristic of past WNP TC track density (Figs. 4a,b) that is also captured fairly well by the explicitly simulated TCs, both from the historical (Figs. 9a,b) and projection simulations (Figs. 10a,b), is the distinctly separated maxima on the eastern and western flanks of the northern Philippines. This characteristic is not as clearly captured in the track density downscaled from reanalysis (Figs. 13a,b) and is only marginally present in the projected track density (Figs. 15a,b). The maximum to the east of the northern Philippines is well defined, which demonstrates that the downscaled TCs tend to spend relatively less of their lifetimes in the South China Sea, both in the past and projected simulations, than the observed and explicitly simulated TCs. For the downscaled TCs, this is largely caused by the intensity model used by the method, which has difficulty simulating the recovery of storms that have passed over land, as often happens when storms pass over the Philippines en route to the South China Sea. As a side note, this stands in contrast to the simulated TCs of Mei et al. (2015), which display a similar minimum of track density in the South China Sea, but due to a substantial dearth of TC genesis in the region.

5. Summary and discussion

There is some general consistency in the past and projected changes in WNP ϕ_{LMI} and the associated changes in TC exposure, although differences exist in the various data considered here. Past observed changes in the period 1980–2013 show a fairly uniform poleward shift in the distribution of ϕ_{LMI}, which manifests in large

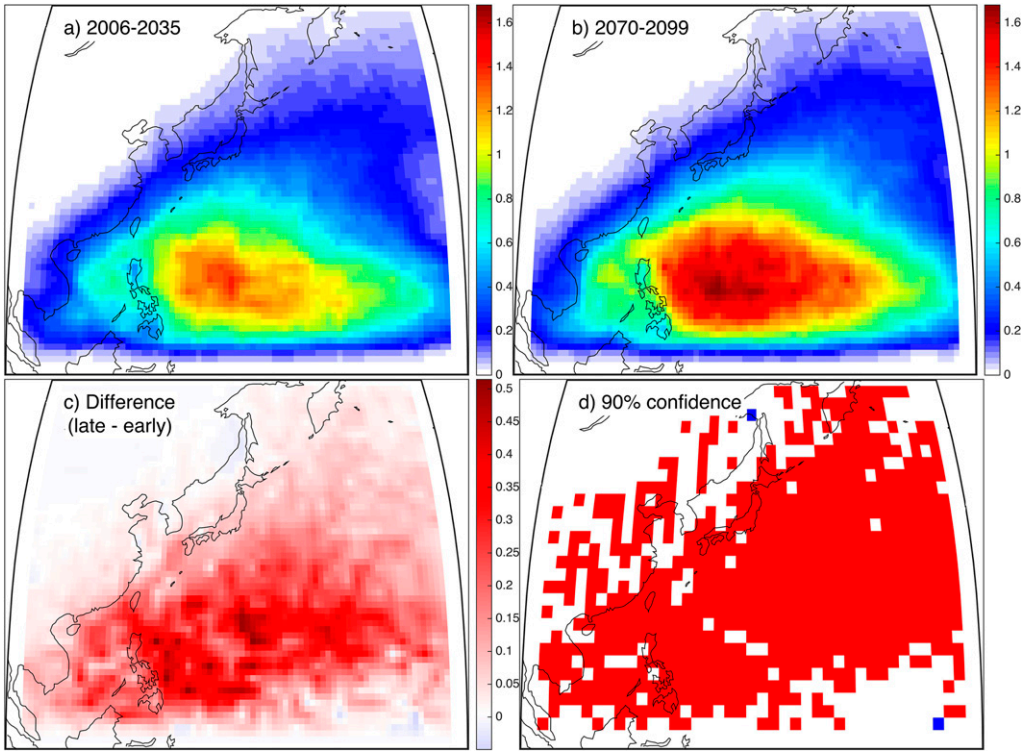

FIG. 14. As in Fig. 4, but for ensemble changes in TC track density in the WNP downscaled from the eight CMIP5 projections in the first and last 30 years of the twenty-first century.

changes in the tails of the distribution (i.e., in the deep tropics and subtropics) and large changes in regional patterns of TC exposure. Decreased exposure is observed in the regions of the Philippine and South China Seas, including the Marianas, the Philippines, Vietnam, and southern China, and increased exposure is observed in the region of the East China Sea, including Japan and its Ryukyu Islands, the Korea Peninsula, and parts of eastern China. Decreases of 50% or more and increases of 100% or more are observed in some regions. These changes result from a combination of basinwide TC frequency decreases (about a 15% decrease in this period) and a robust and significant poleward migration of ϕ_{LMI} of about $0.56^\circ \pm 0.40^\circ$ decade^{-1}. In particular, this combination of factors has a compounding effect at lower latitudes (frequency decreases in concert with track shifts away from the region) and an offsetting effect at higher latitudes (frequency decreases in concert with track shifts into the region). In the latter case, some regions have experienced an increase in exposure as the effect of the track shifts has dominated the effects of reduced basinwide frequency.

For TCs explicitly simulated in the CMIP5 historical simulations, the models substantially underestimate basinwide TC frequency (producing fewer than 6 yr^{-1} in an ensemble average, compared to about 25 yr^{-1} observed) and the poleward migration of ϕ_{LMI} is underestimated and statistically insignificant ($0.3^\circ \pm 0.8^\circ$ decade^{-1}). Still, the general pattern and patterns of change of TC exposure in the historical simulations share a number of similarities to the observed patterns described above. For the TCs downscaled from reanalysis data, the poleward migration rate of ϕ_{LMI} is somewhat underestimated but significant (about $0.4^\circ \pm 0.3^\circ$ decade^{-1}). The patterns of TC exposure, however, do not adequately capture the substantial maximum observed in the South China Sea, in the region west of the Philippines, which makes the patterns of exposure change for the downscaled TCs in that region somewhat suspect.

Twenty-first-century projections of TCs, both explicitly generated within the CMIP5 models and downscaled from CMIP5 model output, identify a continued significant poleward migration of ϕ_{LMI} ($0.2^\circ \pm 0.1^\circ$ and $0.13^\circ \pm 0.04^\circ$ decade^{-1}, respectively) and associated changes in TC exposure patterns that share some similarities with past changes. However, while the explicitly generated TCs decrease in annual basinwide frequency over the twenty-first century, the frequency of downscaled TCs increases, which leads to substantially different projections of TC exposure. For projections based on

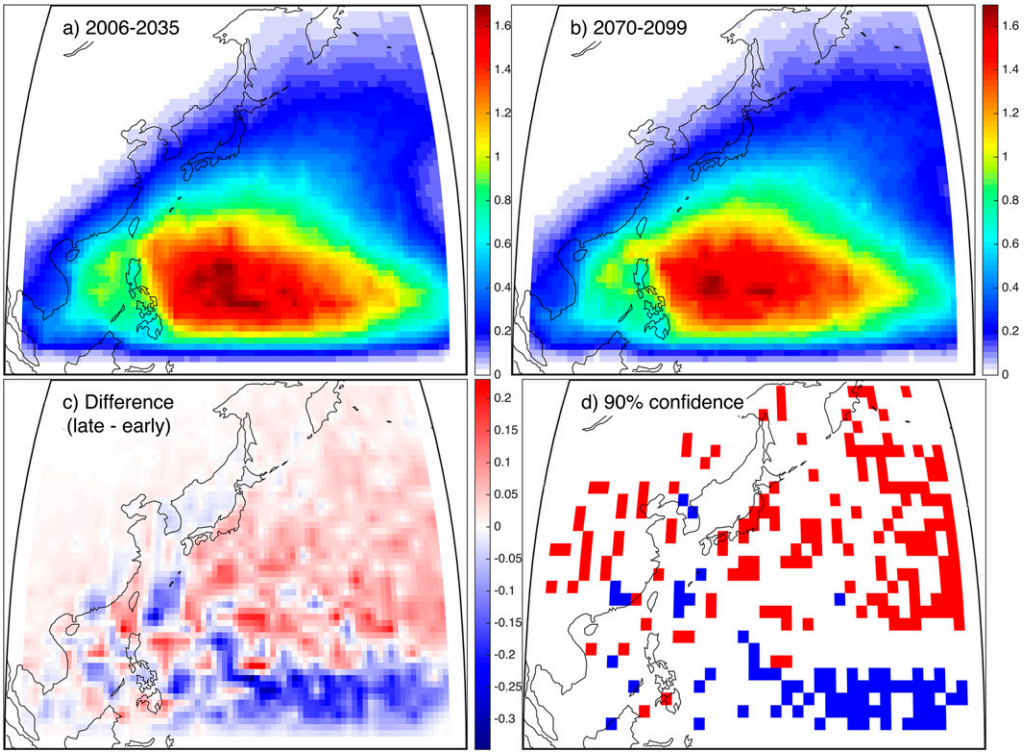

FIG. 15. As in Fig. 14, but for annual frequency fixed to isolate the effect of track changes. Here we used the full sample of 100 synthetic TCs per year.

the downscaled TCs, the exposure increases across the entire basin as the increased frequency dominates the effect of the track changes. The question, then, of how WNP TC frequency will change in the present century is critical to address from the standpoint of regional preparations for changes in TC exposure, particularly in the more southern regions of the WNP basin where the sign of the exposure changes can switch between negative and positive.

The twenty-first-century projections discussed here are based on the RCP8.5 emissions scenario and provide evidence that continued anthropogenic climate forcing can manifest in a continued poleward migration of WNP TC tracks. This is consistent with our analysis of extended time series of historical best-track data over the past ~70 years in which indices of ENSO and the PDO were removed via multiple regression. In this case, the poleward migration rates found in the best-track data from multiple sources remain statistically significant and on the order of about $0.2^\circ\,\text{decade}^{-1}$. The residual migration rate after removing ENSO and PDO variability suggests that the migration has been occurring outside of the dominant known modes of variability in the region, which provides further evidence for an anthropogenic contribution.

While the poleward migration of WNP TCs is projected to occur in concert with basinwide frequency changes (of either sign), the associated changes in regional TC exposure should also be considered in concert with projected increases in TC intensity (Christensen et al. 2013; Peduzzi et al. 2012), which has the potential to further compound changes in regional human mortality risk. Another factor that should be considered is the potential for track changes to affect potable water supplies in some regions that depend on TC passage for their freshwater supplies. But perhaps the greatest potential threat from the changes in TC exposure discussed here lies in the potential for shifting patterns of exposure relative to patterns of sensitivity and resilience. The benefits of reduced TC exposure to regions that are comparatively insensitive and resilient to TC hazards because of past prolonged exposure (e.g., the Marianas) would likely not be as great as the consequences of increased exposure in regions that are more sensitive because of historically less frequent exposure to TC hazards (e.g., Japan and the Korea Peninsula). The known weak bias in the CMIP5 models' ability to simulate the observed tropical expansion should also be considered, as the future migration rate and associated changes in TC exposure could be larger than shown here.

The representative concentration pathway used here (RCP8.5) is based on a presumption of little to no change from the present trajectories of greenhouse gas concentrations (sometimes colloquially referred to as ''business as usual''). The potential for continued changes in regional TC exposure and human mortality risk demonstrated here could tenably be reduced, and even reversed, by changes in emissions standards.

Acknowledgments. JPK is supported by the National Oceanic and Atmospheric Administration National Centers for Environmental Information (NOAA/NCEI). KAE acknowledges support from National Science Foundation Grant 1461517 and Office of Naval Research Grant N000140910526. SJC acknowledges support from NOAA Grant NA110AR4310093 and National Science Foundation Grant AGS-1143959.

REFERENCES

Allen, R. J., J. R. Norris, and M. Kovilakam, 2014: Influence of anthropogenic aerosols and the Pacific decadal oscillation on tropical belt width. *Nat. Geosci.*, **7**, 270–274, doi:10.1038/ngeo2091.

Bell, R., J. Strachan, P. L. Vidale, K. Hodges, and M. Roberts, 2013: Response of tropical cyclones to idealized climate change experiments in a global high-resolution coupled general circulation model. *J. Climate*, **26**, 7966–7980, doi:10.1175/JCLI-D-12-00749.1.

Boo, K.-O., B. B. B. Booth, Y.-H. Byun, J. Lee, C. H. Cho, S. Shim, and K.-T. Kim, 2015: Influence of aerosols in multidecadal SST variability simulations over the North Pacific. *J. Geophys. Res. Atmos.*, **120**, 517–531, doi:10.1002/2014JD021933.

Camargo, S. J., 2013: Global and regional aspects of tropical cyclone activity in the CMIP5 models. *J. Climate*, **26**, 9880–9902, doi:10.1175/JCLI-D-12-00549.1.

——, and A. A. Wing, 2016: Tropical cyclones in climate models. *Wiley Interdiscip. Rev.: Climate Change*, **7**, 211–237, doi:10.1002/wcc.373.

——, A. W. Robertson, S. J. Gaffney, P. Smyth, and M. Ghil, 2007: Cluster analysis of typhoon tracks. Part II: Large-scale circulation and ENSO. *J. Climate*, **20**, 3654–3676, doi:10.1175/JCLI4203.1.

——, ——, A. G. Barnston, and M. Ghil, 2008: Clustering of eastern North Pacific tropical cyclone tracks: ENSO and MJO effects. *Geochem. Geophys. Geosyst.*, **9**, Q06V05, doi:10.1029/2007GC001861.

Cardona, O. D., and Coauthors, 2012: Determinants of risk: Exposure and vulnerability. *Managing the Risks of Extreme Events and Disasters to Advance Climate Change Adaptation*, C. B. Field et al., Eds., Cambridge University Press, 65–108.

Christensen, J. H., and Coauthors, 2013: Climate phenomena and their relevance for future regional climate change. *Climate Change 2013: The Physical Science Basis*, T. F. Stocker et al., Eds., Cambridge University Press, 1217–1308.

Chu, P.-S., J.-H. Kim, and Y. R. Chen, 2012: Have steering flows in the western North Pacific and the South China Sea changed over the last 50 years? *Geophys. Res. Lett.*, **39**, L10704, doi:10.1029/2012GL051709.

Colbert, A. J., B. J. Soden, and B. P. Kirtman, 2015: The impact of natural and anthropogenic climate change on western North Pacific tropical cyclone tracks. *J. Climate*, **28**, 1806–1823, doi:10.1175/JCLI-D-14-00100.1.

Dee, D. P., and Coauthors, 2011: The ERA-Interim reanalysis: Configuration and performance of the data assimilation system. *Quart. J. Roy. Meteor. Soc.*, **137**, 553–597, doi:10.1002/qj.828.

Dong, L., T. Zhou, and X. Chen, 2014: Changes of Pacific decadal variability in the twentieth century driven by internal variability, greenhouse gases, and aerosols. *Geophys. Res. Lett.*, **41**, 8570–8577, doi:10.1002/2014GL062269.

Elsner, J. B., J. P. Kossin, and T. H. Jagger, 2008: The increasing intensity of the strongest tropical cyclones. *Nature*, **455**, 92–95, doi:10.1038/nature07234.

Emanuel, K., 2010: Tropical cyclone activity downscaled from NOAA-CIRES reanalysis, 1908–1958. *J. Adv. Model. Earth Syst.*, **2**, doi:10.3894/JAMES.2010.2.1.

——, 2013: Downscaling CMIP5 climate models shows increased tropical cyclone activity over the 21st century. *Proc. Natl. Acad. Sci. USA*, **110**, 12 219–12 224, doi:10.1073/pnas.1301293110.

——, 2015: Effect of upper-ocean evolution on projected trends in tropical cyclone activity. *J. Climate*, **28**, 8165–8170, doi:10.1175/JCLI-D-15-0401.1.

——, S. Ravela, E. Vivant, and C. Risi, 2006: A statistical deterministic approach to hurricane risk assessment. *Bull. Amer. Meteor. Soc.*, **87**, 299–314, doi:10.1175/BAMS-87-3-299.

——, R. Sundararajan, and J. Williams, 2008: Hurricanes and global warming: Results from downscaling IPCC AR4 simulations. *Bull. Amer. Meteor. Soc.*, **89**, 347–367, doi:10.1175/BAMS-89-3-347.

Goh, A. Z.-C., and J. C. L. Chan, 2012: Variations and prediction of the annual number of tropical cyclones affecting Korea and Japan. *Int. J. Climatol.*, **32**, 178–189, doi:10.1002/joc.2258.

Ho, C.-H., J.-J. Baik, J.-H. Kim, D.-Y. Gong, and C.-H. Sui, 2004: Interdecadal changes in summertime typhoon tracks. *J. Climate*, **17**, 1767–1776, doi:10.1175/1520-0442(2004)017<1767:ICISTT>2.0.CO;2.

Horn, M., and Coauthors, 2014: Tracking scheme dependence of simulated tropical cyclone response to idealized climate simulations. *J. Climate*, **27**, 9197–9213, doi:10.1175/JCLI-D-14-00200.1.

Hu, Y. Y., L. J. Tao, and J. P. Liu, 2013: Poleward expansion of the Hadley circulation in CMIP5 simulations. *Adv. Atmos. Sci.*, **30**, 790–795, doi:10.1007/s00376-012-2187-4.

Jiang, H., and E. Zipser, 2010: Contribution of tropical cyclones to the global precipitation from eight seasons of TRMM data: Regional, seasonal, and interannual variations. *J. Climate*, **23**, 1526–1543, doi:10.1175/2009JCLI3303.1.

Kalnay, E., and Coauthors, 1996: The NCEP/NCAR 40-Year Reanalysis Project. *Bull. Amer. Meteor. Soc.*, **77**, 437–471, doi:10.1175/1520-0477(1996)077<0437:TNYRP>2.0.CO;2.

Kang, N.-Y., and J. B. Elsner, 2016: Climate mechanism for stronger typhoons in a warmer world. *J. Climate*, **29**, 1051–1057, doi:10.1175/JCLI-D-15-0585.1.

Knapp, K. R., M. C. Kruk, D. H. Levinson, H. J. Diamond, and C. J. Neumann, 2010: The International Best Track Archive for Climate Stewardship (IBTrACS). *Bull. Amer. Meteor. Soc.*, **91**, 363–376, doi:10.1175/2009BAMS2755.1.

Kossin, J. P., S. J. Camargo, and M. Sitkowski, 2010: Climate modulation of North Atlantic hurricane tracks. *J. Climate*, **23**, 3057–3076, doi:10.1175/2010JCLI3497.1.

——, T. L. Olander, and K. R. Knapp, 2013: Trend analysis with a new global record of tropical cyclone intensity. *J. Climate*, **26**, 9960–9976, doi:10.1175/JCLI-D-13-00262.1.

——, K. A. Emanuel, and G. A. Vecchi, 2014: The poleward migration of the location of tropical cyclone maximum intensity. *Nature*, **509**, 349–352, doi:10.1038/nature13278.

Lam, H., M. H. Kok, and K. K. Y. Shum, 2012: Benefits from typhoons—The Hong Kong perspective. *Weather*, **67**, 16–21, doi:10.1002/wea.836.

Li, T., M. Kwon, M. Zhao, J.-S. Kug, J.-J. Luo, and W. Yu, 2010: Global warming shifts Pacific tropical cyclone location. *Geophys. Res. Lett.*, **37**, L21804, doi:10.1029/2010GL045124.

Lin, I.-I., and J. Chan, 2015: Recent decrease in typhoon destructive potential and global warming implications. *Nat. Commun.*, **6**, 7182, doi:10.1038/ncomms8182.

Liu, K. S., and J. C. L. Chan, 2008: Interdecadal variability of western North Pacific tropical cyclone tracks. *J. Climate*, **21**, 4464–4476, doi:10.1175/2008JCLI2207.1.

——, and ——, 2013: Inactive period of western North Pacific tropical cyclone activity in 1998–2011. *J. Climate*, **26**, 2614–2630, doi:10.1175/JCLI-D-12-00053.1.

Lucas, C., B. Timbal, and H. Nguyen, 2014: The expanding tropics: A critical assessment of the observational and modeling studies. *Wiley Interdiscip. Rev.: Climate Change*, **5**, 89–112, doi:10.1002/wcc.251.

Manganello, J. V., and Coauthors, 2014: Future changes in the western North Pacific tropical cyclone activity projected by a multidecadal simulation with a 16-km global atmospheric GCM. *J. Climate*, **27**, 7622–7646, doi:10.1175/JCLI-D-13-00678.1.

Mantua, N. J., S. R. Hare, Y. Zhang, J. M. Wallace, and R. C. Francis, 1997: A Pacific interdecadal climate oscillation with impacts on salmon production. *Bull. Amer. Meteor. Soc.*, **78**, 1069–1079, doi:10.1175/1520-0477(1997)078<1069:APICOW>2.0.CO;2.

Martin, J. D., and W. M. Gray, 1993: Tropical cyclone observation and forecasting with and without aircraft reconnaissance. *Wea. Forecasting*, **8**, 519–532, doi:10.1175/1520-0434(1993)008<0519:TCOAFW>2.0.CO;2.

Meehl, G. A., A. Hu, J. M. Arblaster, J. Fasullo, and K. E. Trenberth, 2013: Externally forced and internally generated decadal climate variability associated with the interdecadal Pacific oscillation. *J. Climate*, **26**, 7298–7310, doi:10.1175/JCLI-D-12-00548.1.

Mei, W., S.-P. Xie, and M. Zhao, 2014: Variability of tropical cyclone track density in the North Atlantic: Observations and high-resolution simulations. *J. Climate*, **27**, 4797–4814, doi:10.1175/JCLI-D-13-00587.1.

——, ——, ——, and Y. Wang, 2015: Forced and internal variability of tropical cyclone track density in the western North Pacific. *J. Climate*, **28**, 143–167, doi:10.1175/JCLI-D-14-00164.1.

Mori, M., and Coauthors, 2013: Hindcast prediction and near-future projection of tropical cyclone activity over the western North Pacific using CMIP5 near-term experiments with MIROC. *J. Meteor. Soc. Japan*, **91**, 431–452, doi:10.2151/jmsj.2013-402.

Murakami, H., B. Wang, and A. Kitoh, 2011: Future change of western North Pacific typhoons: Projections by a 20-km-mesh global atmospheric model. *J. Climate*, **24**, 1154–1169, doi:10.1175/2010JCLI3723.1.

——, and Coauthors, 2012: Future changes in tropical cyclone activity projected by the new high-resolution MRI-AGCM. *J. Climate*, **25**, 3237–3260, doi:10.1175/JCLI-D-11-00415.1.

Nguyen, H., C. Lucas, A. Evans, B. Timbal, and L. Hanson, 2015: Expansion of the Southern Hemisphere Hadley cell in response to greenhouse gas forcing. *J. Climate*, **28**, 8067–8077, doi:10.1175/JCLI-D-15-0139.1.

Peduzzi, P., B. Chatenoux, H. Dao, A. De Bono, C. Herold, J. Kossin, F. Mouton, and O. Nordbeck, 2012: Tropical cyclones: Global trends in human exposure, vulnerability and risk. *Nat. Climate Change*, **2**, 289–294, doi:10.1038/nclimate1410.

Ramsay, H. A., S. J. Camargo, and D. Kim, 2012: Cluster analysis of tropical cyclone tracks in the Southern Hemisphere. *Climate Dyn.*, **39**, 897–917, doi:10.1007/s00382-011-1225-8.

Rayner, N. A., D. E. Parker, E. B. Horton, C. K. Folland, L. V. Alexander, D. P. Rowell, E. C. Kent, and A. Kaplan, 2003: Global analyses of sea surface temperature, sea ice, and night marine air temperature since the late nineteenth century. *J. Geophys. Res.*, **108**, 4407, doi:10.1029/2002JD002670.

Riahi, K., and Coauthors, 2011: RCP 8.5—A scenario of comparatively high greenhouse gas emissions. *Climatic Change*, **109**, 33–57, doi:10.1007/s10584-011-0149-y.

Rienecker, M., and Coauthors, 2011: MERRA: NASA's Modern-Era Retrospective Analysis for Research and Applications. *J. Climate*, **24**, 3624–3648, doi:10.1175/JCLI-D-11-00015.1.

Roberts, M. J., and Coauthors, 2015: Tropical cyclones in the UPSCALE ensemble of high-resolution global climate models. *J. Climate*, **28**, 574–596, doi:10.1175/JCLI-D-14-00131.1.

Taylor, K. E., R. J. Stouffer, and G. A. Meehl, 2012: A summary of the CMIP5 experiment design. *Bull. Amer. Meteor. Soc.*, **93**, 485–498, doi:10.1175/BAMS-D-11-00094.1.

Walsh, K. J. E., and Coauthors, 2015: Hurricanes and climate: The U.S. CLIVAR working group on hurricanes. *Bull. Amer. Meteor. Soc.*, **96**, 997–1017, doi:10.1175/BAMS-D-13-00242.1.

Wang, C., and X. Wang, 2013: Classifying El Niño Modoki I and II by different impacts on rainfall in southern China and typhoon tracks. *J. Climate*, **26**, 1322–1338, doi:10.1175/JCLI-D-12-00107.1.

——, and L. G. Wu, 2015: Influence of future tropical cyclone track changes on their basin-wide intensity over the western North Pacific: Downscaled CMIP5 projections. *Adv. Atmos. Sci.*, **32**, 613–623, doi:10.1007/s00376-014-4105-4.

Wang, R., L. Wu, and C. Wang, 2011: Typhoon track changes associated with global warming. *J. Climate*, **24**, 3748–3752, doi:10.1175/JCLI-D-11-00074.1.

Wu, L., and B. Wang, 2004: Assessment of global warming impacts on tropical cyclone track. *J. Climate*, **17**, 1686–1698, doi:10.1175/1520-0442(2004)017<1686:AIOGWO>2.0.CO;2.

——, and Coauthors, 2014: Simulations of the present and late-twenty-first-century western North Pacific tropical cyclone activity using a regional model. *J. Climate*, **27**, 3405–3424, doi:10.1175/JCLI-D-12-00830.1.

Yokoi, S., and Y. N. Takayabu, 2013: Attribution of decadal variability in tropical cyclone passage frequency over the western North Pacific: A new approach emphasizing the genesis location of cyclones. *J. Climate*, **26**, 973–987, doi:10.1175/JCLI-D-12-00060.1.

——, ——, and H. Murakami, 2013: Attribution of projected future changes in tropical cyclone passage frequency over the western North Pacific. *J. Climate*, **26**, 4096–4111, doi:10.1175/JCLI-D-12-00218.1.

Zhang, W., H.-F. Graf, Y. Leung, and M. Herzog, 2012: Different El Niño types and tropical cyclone landfall in East Asia. *J. Climate*, **25**, 6510–6523, doi:10.1175/JCLI-D-11-00488.1.

Zhao, H., and L. Wu, 2014: Inter-decadal shift of the prevailing tropical cyclone tracks over the western North Pacific and its mechanism study. *Meteor. Atmos. Phys.*, **125**, 89–101, doi:10.1007/s00703-014-0322-8.

——, ——, and W. Zhou, 2010: Assessing the influence of the ENSO on tropical cyclone prevailing tracks in the western North Pacific. *Adv. Atmos. Sci.*, **27**, 1361–1371, doi:10.1007/s00376-010-9161-9.